Coupled effect of crystallographic orientation and indenter geometry on nanoindentation of single crystalline copper

Zhanfeng Wang , Junjie Zhang , Hamad ul Hassan , Jianguo Zhang , Yongda Yan , Alexander Hartmaier , Tao Sun

PII: S0020-7403(18)31368-7
DOI: https://doi.org/10.1016/j.ijmecsci.2018.09.007
Reference: MS 4506

To appear in: *International Journal of Mechanical Sciences*

Received date: 28 April 2018
Revised date: 12 August 2018
Accepted date: 5 September 2018

Please cite this article as: Zhanfeng Wang , Junjie Zhang , Hamad ul Hassan , Jianguo Zhang , Yongda Yan , Alexander Hartmaier , Tao Sun , Coupled effect of crystallographic orientation and indenter geometry on nanoindentation of single crystalline copper, *International Journal of Mechanical Sciences* (2018), doi: https://doi.org/10.1016/j.ijmecsci.2018.09.007

Highlights

- CPFEM simulation data of Berkovich nanoindentation quantitatively agrees with experimental results;
- A coupled effect of crystallographic orientation and indenter geometry is revealed and analyzed;
- A pile-up density factor is proposed to qualitatively characterize pile-up deformation behavior.

Coupled effect of crystallographic orientation and indenter geometry on nanoindentation of single crystalline copper

Zhanfeng Wang[1], Junjie Zhang[1,*], Hamad ul Hassan[2], Jianguo Zhang[3], Yongda Yan[1], Alexander Hartmaier[2], Tao Sun[1]

[1]Center for Precision Engineering, Harbin Institute of Technology, Harbin 150001, China

[2]Interdisciplinary Centre for Advanced Materials Simulation, Ruhr-University Bochum, Bochum 44780, Germany

[3]Department of Aerospace Engineering, Nagoya University, Nagoya 4648603, Japan

Corresponding author: zhjj505@gmail.com (JZ)

Abstract: Surface pile-up topography is very significant for property extraction in nanoindentation tests. In the present work, we perform crystal plasticity finite element simulations of Berkovich nanoindentation of single crystalline copper with different crystallographic orientations, which derive quantitatively comparable mechanical properties and surface pile-up topographies with experimental data. Simulation results demonstrate that there is a coupled effect of crystallographic orientation of indented material and indenter geometry on surface pile-up behavior, due to the interaction between intrinsic dislocation slip events and extrinsic discrete stress distribution patterns. Based on the relative spatial orientation between crystallographic orientation of indented material and indenter geometry, a surface pile-up density factor m_p is proposed to qualitatively characterize the propensity of surface pile-up behaviour in nanoindentation tests of single crystalline copper.

Keywords: Nanoindentation; single crystalline copper; surface pile-up; indenter geometry; crystal plasticity finite element method.

1 Introduction

Nanoindentation test is a popular technique for extracting mechanical properties of materials at small length scales. In the loading phase of a typical nanoindentation test, the contact area between the indenter

and the target material can be indirectly measured by recording load and penetration depth of the indenter with a known geometry, which leads to estimation of contact pressure and hardness. In the subsequent unloading phase, the elastic modulus of target material can be derived from initial unloading elastic response due to the relaxation of elastic strains within target material [1-2]. In addition, other mechanical properties, such as residual stress [3-4], incipient plasticity [5-6], creep [7], hardening [8], are also central topics in nanoindentation tests for property extraction.

The change of surface topography around the plastic deformation-induced residual impression, i.e., pile-up or sink-in, plays an important role in nanoindentation tests [9]. The change of surface topography greatly influences the measurement of contact area in nanoindentation tests, as well as acts as an effective criterion of mechanical properties of target material, such as the strain-hardening behavior [10-11]. In particular, the symmetry of surface pile-up, which dominates the ejection of strain-hardened material under nanoindentation tests, is an important factor for characterizing the surface pile-up behavior. It has been theoretically and experimentally demonstrated that the symmetry of surface pile-up is a close reflection of the underlying crystal geometry of target material. For instance, both simulations and experiments of nanoindentation tests of single crystalline face-centered cubic (FCC) metals show that the pile-up pattern has a fourfold, twofold, and threefold (or six-fold) symmetry for the (010), (110), and (111) orientation, respectively [12-14]. The influence of crystallographic orientation on the symmetry of surface pile-up has been primarily attributed to the geometry of the activated slip systems with respect to the indented surface [15-17]. However, recent work reported that the indenter geometry also has a significant influence on the surface pile-up pattern, which adds exceptions to the crystallographic orientation-dependent symmetry of surface pile-up. Kucharski et al. reported that the pile-up pattern of single crystal copper under Berkovich nanoindentation tests primarily depends on the indenter geometry at small load, rather than dominantly correlates with the crystallographic orientation of target material at large load [18]. Yao et al. found that the pile-up pattern of Berkovich indentation did not necessarily reflect the rotational crystal symmetry of tungsten single crystal specimen. For instance, only three hillocks formed on the (100) surface, which is essentially affected by the sharp edges of the indenter [19]. Renner et al. reported that the Berkovich indenter orientation in a given indented plane also significantly influences the pile-up distribution of nickel,

in addition to the crystallographic orientation of target material [20]. The modification of the original crystallographic orientation-dependent symmetry of surface pile-up by the indenter geometry in Berkovich nanoindentation tests can be attributed to the discrete stress distribution pattern built by the polygonal side edges of the indenter. Therefore, it is also of significant importance to investigate the influence of indenter geometry on the symmetry of surface pile-up in nanoindentation tests.

The crystal plasticity finite element method (CPFEM), acting as an important supplementary for experimental investigations, has also been widely employed to explore the surface pile-up deformation behavior in nanoindentation tests [21-23]. However, most of previous CPFEM studies reported that the surface pile-up pattern in nanoindentation tests is solely determined by crystallographic processes. Recent CPFEM simulations by Yao et al. [19] and Renner et al. [20] successfully captured the effect of Berkovich indenter geometry on the symmetry of surface pile-up. They reported that the surface pile-up distribution is strongly related to the indented crystallographic orientation and to the indenter orientation in a given indented plane, which can be attributed the slip trace on the 12 slip systems of FCC metals at the maximum indentation depth. However, the activation of dominant slip systems for the formation of different pile-up patterns under different crystallographic orientations is not analysed. Furthermore, although the load-displacement curves obtained in previous CPFEM studies of nanoindentation tests are in good quantitative agreement with experiments, the quantitative comparison of surface pile-up topography between CPFEM simulations and experiments is still challenging due to the proper selection of hardening model in CPFEM simulations. The hardening model proposed by Brown et al. [24] and Kalidindi et al. [25], which is most widely used in previous CPFEM studies, is a constitutive law based on hardening rate of single slip. Lin and Havner [26] comparatively studied five hardening models used in CPFEM simulations of torsion test of polycrystalline copper, and concluded that the hardening model proposed by Bassani and Wu [27] possesses the best prediction accuracy in terms of aggregate shear stress-strain curves, evolving crystallographic textures, yield loci, and axial stresses. Therefore, the rational selection of employed hardening model is critical for the characterization of surface pile-up in CPFEM simulations of nanoindentation tests.

In the present work, we perform 3D CPFEM studies of Berkovich nanoindentation tests of single crystalline copper with different crystallographic orientations, with an emphasis on evaluating the coupled effect of the crystallographic orientation of target material and the indenter geometry on the surface pile-up behaviour. High resolution electron back-scatter diffraction (EBSD) characterization technique is employed to measure the distribution of the crystallographic orientation of target materials. The comparison between simulation data and experimental results in terms of load-displacement curves and surface pile-up topography is carried out. Finally, a factor representing the formation propensity of surface pile-up is proposed to qualitatively characterize surface pile-up topography.

2 Methods

2.1 CPFEM model of nanoindentation test

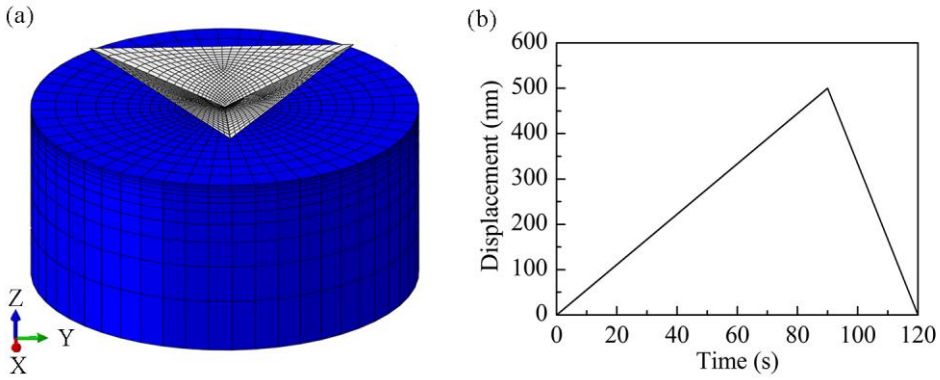

Fig. 1 Configuration of CPFEM simulation of nanoindentation test. (a) 3D nanoindentation model; (b) Scheme of loading and unloading phases

Fig. 1(a) shows the 3D CPFEM model of nanoindentation test, which consists of a cylindrical copper specimen and a Berkovich diamond indenter. The cylindrical specimen has a diameter of 10 μm and a height of 5 μm, which is meshed by 14300 eight-node linear brick elements (C3D8) and 572 linear wedge elements (C3D6). The C3D6 elements are distributed around the axis of the cylindrical specimen to avoid the effect of mesh symmetry. The C3D6 element size gradually transits from the minimum value of 28 nm in the centre to the maximum value of 625 nm at the edge of the cylinder. The Berkovich indenter with a tip radius of 60 nm is meshed by 1434 discrete rigid elements (R3D4) with a minimum element size of 10 nm.

Three indented surfaces of different crystallographic orientations, as (010)-, (110)-, and (111)-oriented, are considered. The crystallographic orientation of simulated specimen is set in the way of Euler angles (Ψ1 φ Ψ2), which are derived from the EBSD characterization of according single crystalline copper specimen. Specifically, the Z and X axis is parallel to the [hkl] and [uvw] orientation, respectively. Fig. 1(b) shows the scheme of loading and unloading phases in the displacement-controlled nanoindentation tests. In the loading phase, the indenter penetrates into the specimen with a constant velocity of 5.56 nm/s until it reaches a pre-determined depth of 500 nm. In the following unloading stage, the indenter is withdrawn from the specimen with a constant velocity of 16.67 nm/s. The friction coefficient between the copper specimen and the diamond indenter is 0.1. It should be noted that in the current CPFEM model, the ratio of the specimen height to the maximum penetration depth is 10 to reduce computational costs for UMAT calculation. A higher ratio of 20 is also checked, which shows negligible difference in the mechanical response with that of the ratio of 10.

The as-created 3D CPFEM model of nanoindentation test is constructed by the implicit finite element code ABAQUS, based on the integration of crystal plasticity constitutive model in the UMAT user subroutine. The principle of single-crystal plasticity is detailed described in Refs. [28-34] and formulated in Refs. [35-36]. The formulation of the UMAT used in this work follows the typical theoretical framework presented by Asaro et al. [33, 37]. More details about the formulating of elastic-plastic single crystal deformation can be found elsewhere [38-40].

It is known that the plasticity of crystalline metallic materials is governed by dislocation slip. In particular for FCC crystals, there are 12 slip systems under the permutations of {111} slip planes and <110> slip directions. Dislocation slip is triggered when the shear stress on a slip plane reaches the critical resolved shear stress (CRSS) under the Schmid's law. Following the Boeff definition [41], the CRSS on a specific slip system can be established by determining the Cauchy stress vectors, which are then projected in slip directions. In the finite strain framework, the second Piola-Kirchhoff stress in intermediate configuration is used to determine the resolved shear stress. To characterize the mobility of dislocation motion, the constitutive variable of slip rate $\dot{\gamma}^{\alpha}$ is defined as [42]:

$$\dot{\gamma}^{\alpha}=\dot{\gamma}_0\left|\frac{\tau^{\alpha}}{\tau_c^{\alpha}}\right|^{m} sign\left(\tau^{\alpha}\right) \tag{1}$$

Where τ_c^{α} is the work hardening-dependent CRSS, τ^{α} is the resolved shear stress, $\dot{\gamma}_0$ is the reference shear rate and m is the power law exponent. The sessile dislocation structures formed by dislocation reaction and cross-slip events act as barriers to impede subsequent dislocation motion, which leads to strain hardening occurred within the material accompanied with increased yield stress. Accordingly, the hardening rule employed in the CPFEM model should accurately specify the relationship between the work hardening-dependent CRSS τ_c^{α} and the plastic strain. At time t=0, each slip system has the same initial CRSS $\tau_{c_0}^{\alpha}$. However, the strength of activated slip systems increases with plastic shear strain [43], which can be well characterized by the hardening rule defined by Bassani and Wu [27]:

$$\dot{\tau}_c^{\alpha}=\sum_{\beta=1}^{N_s} h_{\alpha\beta}\left|\dot{\gamma}^{\beta}\right| \tag{2}$$

Where $h_{\alpha\beta}$ is the hardening matrix, which is defined as:

$$h_{\alpha\beta}=h_0\left(1-\frac{\tau_c^{\alpha}}{\tau_s}\right)^{n} q_{\alpha\beta} \tag{3}$$

Where h_0 is the hardening matrix at time t=0, n is hardening factor, τ_s is the saturated shear stress. The parameter $q_{\alpha\beta}$ is a measurement of latent hardening between slip systems α and β that renders the hardening model anisotropic. The value of this latent hardening is 1.0 and 1.4 for coplanar and non-coplanar slip systems, respectively [44]. Table. 1 lists the detailed mechanical parameters used in the constitutive model. The values of those parameters are first set to the values presented by Eidel [45], and then modified by fitting the simulated load-displacement curve with experimental one in nanoindentation of single crystalline copper. Specifically, two nanoindentation events are first performed, and the load-displacement curves in the loading stage are then fitted with that obtained by CPFE simulations. The two sets of derived parameters are then averaged to obtain the final set of parameters for the constitutive model.

Table. 1 Mechanical parameters of single crystalline copper employed in the constitutive model.

	Parameter	C11	C12	C44	nslip	m	$\dot{\gamma}_0$	h_0	τ_c^α	τ_s	n
CPFEM	value	168.4d3	121.4d3	75.4d3	12	13	1e-9	110	32	100	3

2.2 Experimental setup of nanoindentation

High-purity (99.99%) single crystalline (010)-, (110)-, and (111)-oriented Cu specimens, with in-plane dimensions of 10 mm times 5 mm and thickness of 1 mm, are obtained from the Hefei Kejing Mateials Technology Co., LTD. The surface roughness of the as-received Cu specimens is 5 nm. Fig. 2 shows the inverse pole figures (IPF) obtained from the EBSD characterization of as-received Cu specimens. Table. 2 lists the derived Euler angles (Ψ1 φ Ψ2), which are used to precisely determined the crystallographic orientations of the simulated copper specimens in the CPFEM models.

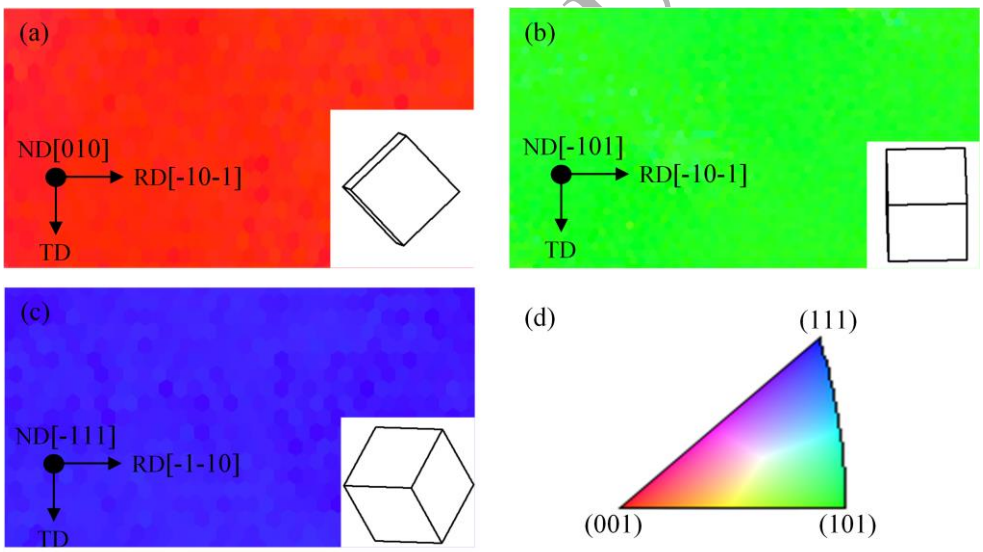

Fig. 2 EBSD IPF mapping of differently oriented surfaces: (a) (010) surface, (b) (-101) surface, (c) (-111) surface, (d) Color coded map type: inverse pole [001] copper.

Table 2 Crystalline orientations of three single crystalline Cu samples

	Euler angles (Ψ1 φ Ψ2)	Miller indices
Sample-1	223.9 92.5 5.3	（0 1 0）[-1 0 -1]
Sample-2	270.4 44.6 271.1	（-1 0 1）[-1 0 -1]
Sample-3	177.7 57.1 318.4	（-1 1 1）[-1 -1 0]

Berkovich nanoindentation experiments are performed on single crystalline Cu specimens using the Keysight Nano Indenter G200. The Berkovich indenter has a flat profile with a total included angle of 142.3 degrees, a half angle of 65.3 degrees and a tip radius of 60 nm. Nanoindentation tests are conducted in the isolated chamber and at room temperature under the continuous stiffness measurement (CSM) mode, which offers a direct measurement of dynamic contact stiffness during the loading phase of an indentation test [30]. In the nanoindentation tests, the indenter first penetrates into the specimen with a constant velocity of 10 nm/s until it reaches a pre-determined depth of 500 nm, and then is withdrawn from the specimen to its initial position before the penetration.

3 Results and discussion

3.1 Mechanical properties

The load-displacement curves obtained in experiments of nanoindentation tests of (010)-, (110)-, and (111)-oriented single crystalline copper are plotted in Fig. 3. For each crystallographic orientation, two repetitive indentation tests are performed to check the reproducibility of results, as well as to control accidental error in the nanoindentation tests. The distance between the two adjacent indentation events is 20 μm. Fig. 3(a) presents the scanning electron microscope (SEM) image of the residual impression on Cu(010), which shows that one edge of the Berkovich indenter is along the TD direction (i.e. the X axis in the simulation model). Being consistent with the experiments, CPFEM simulations of nanoindentation tests are also performed on single crystalline copper with different crystallographic orientations.

Fig. 3(b)-(d) plot load-displacement curves of Cu(010), Cu(110) and Cu(111) by both CPFEM simulations and experiments of nanoindentation tests. Table. 3 lists the derived mechanical properties of copper specimen from CPFEM simulations and experiments of nanoindentation tests. The Hertz contact theory [1] is adopted to derive mechanical properties of the specimen by fitting the portion of simulated load-displacement curve in the loading stage below a displacement of 50 nm, given the known Poisson's ratio of Cu as 0.33, Possion's ratior of diamond as 0.07 and Young's modulus of diamond as 1140 GPa [46]. It is seen from Fig. 3 and Table. 3 that the derived mechanical properties of single crystalline copper from the two repetitive nanoindentation tests are consistent. Furthermore, the experimental results are in good

agreement with CPFEM simulation data. Specifically, both experiments and simulations show that the Young's modulus and Hardness is different for varied crystallographic orientations, and the (111)-oriented copper have the highest Young's modulus. It is also noted that there are also discrepancies existed in the mechanical response between CPFEM simulations and experiments. Firstly, Fig. 3 shows that there is minor derivation in the slopes of loading and unloading phases between experiments and simulations, and the residual displacement in the simulation is higher than that in the experiments for each crystallographic orientation. Secondly, a maximum difference of 15% exists the derived values of both Young's modulus and hardness from simulations and experiments. The as mentioned difference in mechanical response between CPFEM simulations and experiments can be attributed to following aspects. Firstly, there are minor difference in indentation conditions between CPFEM simulations and experiments, in terms of flatness and purity of specimen, geometry of indenter, etc. Secondly, nanoindentation experiments are conducted using a CSM mode, whereas the simulated indentations are conducted in a displacement-control mode, which leads to discrepancy in indentation depth between experiments and CPFEM simulations. Thirdly, the fineness of mesh in the CPFEM simulation also affects simulation results. Fourthly, there could be an influence arising from the employed constitutive law. Fifthly, the unknown frictional conditions might also affect the prediction results.

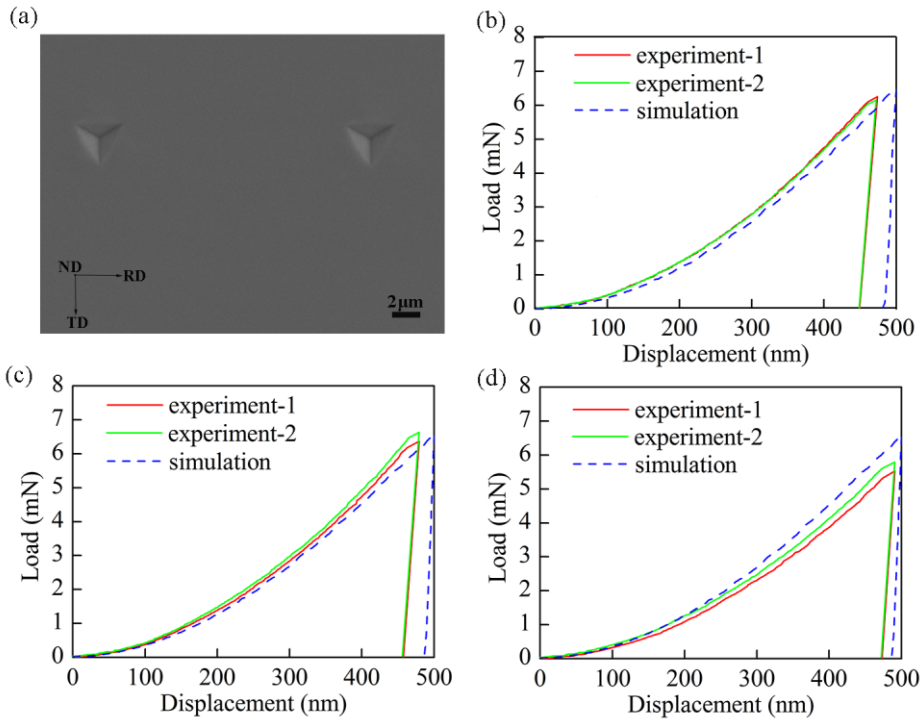

Fig. 3 Mechanical responses of single crystalline copper in nanoindentation tests. (a) SEM image of residual indentation impression of Cu (010); experimental and simulated load-displacement curves of (b) Cu(010), (c) Cu(110) and (d) Cu(111).

Table 3 Mechanical properties of Cu samples from CPFEM simulations and experiments of nanoindentation

		Hardness/GPa	Young's modulus/GPa
(010)	experiment-1	1.33	125.6
	experiment-2	1.33	128.2
	Simulation	1.12	105.4
(-101)	experiment-1	1.46	138.6
	experiment-2	1.50	140.4
	Simulation	1.23	134.4
(-111)	experiment-1	1.26	139.0
	experiment-2	1.14	134.0
	Simulation	1.12	154.7

3.2 Surface pile-up

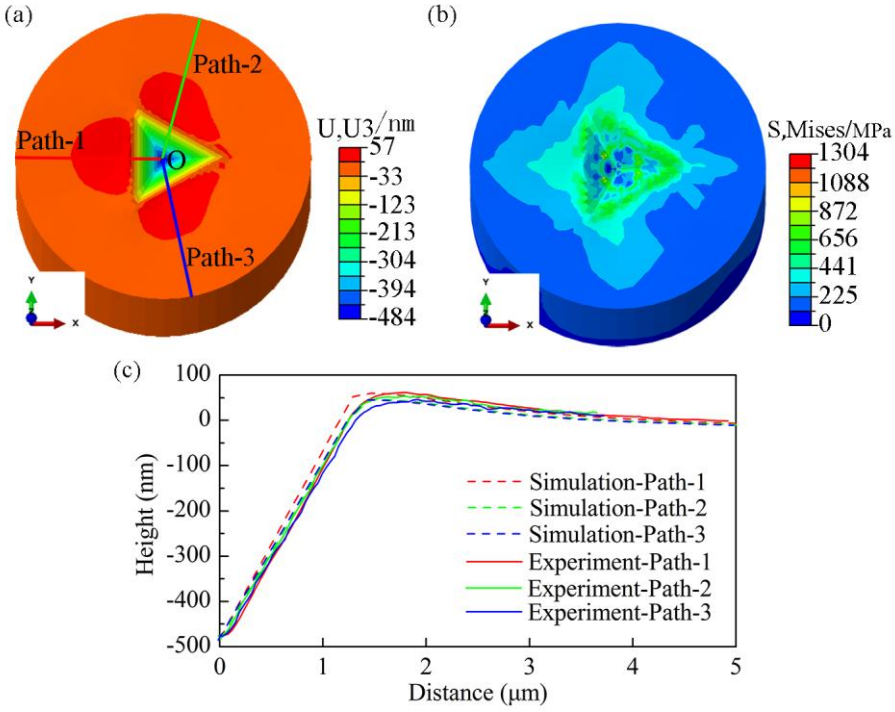

Fig. 4 Surface pile-up topography of Cu(010) after CPFEM simulation of nanoindentation. (a) Residual impression, (b) Mises stress distribution, (c) Surface pile-up height-distance curves.

Fig. 4(a) presents the morphology of Cu(010) after CPFEM simulation of nanoindentation test with a Berkovich indenter (tip radius of 60 nm). It is seen from Fig. 4(a) that there is a triangular residual impression remained on the indented surface. Furthermore, there are pronounced material accumulations around the residual impression, i.e., surface pile-up with a three-fold symmetry formed. Fig. 4(b) further demonstrates that the distribution of Mises stress is closely coincided with the surface pile-up distribution. Fig. 4(b) also indicates that the values of equivalent stress is equal to zero at the base of the specimen, suggesting negligible influence by the utilized ratio of specimen height to penetration depth in current CPFEM model. Although the value of equivalent stress at the outer surface of the specimen is approximately 200 MPa, the adoption of free boundary condition at the outer surface means that there is no reaction force from the element at the external boundary or from the region of interest related to surface pile-up behaviour. As illustrated in Fig. 4(a), three lines with different colours are drawn to cross the three parts of formed surface pile-up, aiming to quantitatively characterize the surface pile-up height. Accordingly, Fig. 4(c) plots the surface pile-up height-distance curves for the three lines, indicating the minor discrepancy in the pile-up height of the three-fold parts represented along different lines. Specifically, the height of surface pile-up along the red line, i.e. TD direction, has a larger value of 57.2 nm than the other two lines. In addition to the CPFEM simulation of Cu(010), the nanoindentation experiment of Cu(010) is also conducted. Fig. 5 shows that the surface pile-up of Cu(010) also presents a three-fold symmetry. It should be noted that the minimum scale value is -200 nm in the AFM images for clear observation of surface pile-up topography. Be similar with the CPFEM simulation shown in the Fig. 4(a), the three parts of surface pile-up after the nanoindentation experiment are characterized by atomic force microscope (AFM). Accordingly, Fig. 4(c) plots the height-distance curves obtained in the nanoindentation experiment, which also shows the same trend with the CPFEM simulation. The maximum surface pile-up height of Cu(010) obtained in nanoindentation experiments is 62.1 nm, which agrees well with the CPFEM simulation result of 57.2 nm.

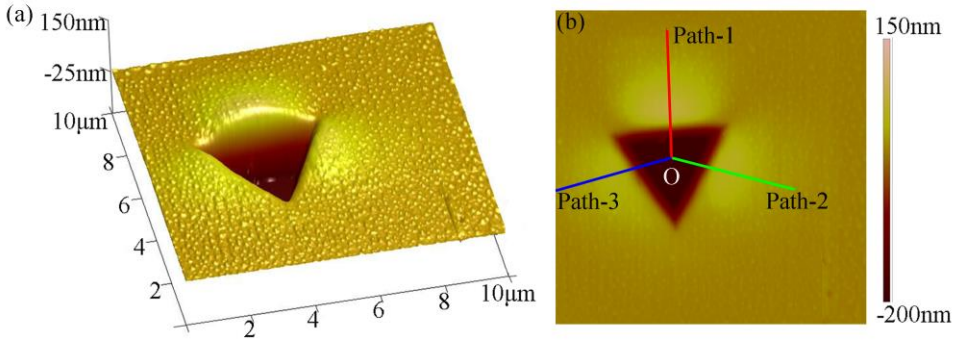

Fig. 5 AFM images of residual impression on Cu(010) after Berkovich nanoindentation experiment. (a) 3D characterization; (b) 2D characterization.

Fig. 6(a)-(c) show the evolution of surface pile-up topography in the CPFEM simulation of nanoindentation of Cu(010), which shows that the characteristic of surface pile-up doesn't change with indentation depth. In particular, it is seen from Fig. 6(a) that at a low displacement of 112 nm, the surface pile-up still has a three-fold symmetry. Furthermore, Fig. 6(d) presents the displacement-time curves of the point "P" marked in the Fig. 6(c) along the minus X axis, Y axis and Z axis. The value along the minus X axis and Z axis represents the distance between the point "P" and the indenter and the pile-up height, respectively. Fig. 6(d) shows that the formation of surface pile-up starts from an indentation time of 30 s, after which the pile-up height increases rapidly. Dynamic examination of simulated indentation process indicates that the plastic deformation in the loading phase can be divided into two sequential stages. In the first stage with an indentation time from 30 s to 50s, the plastic deformation is accompanied with dislocation slip on activated slip systems. In the second stage with an indentation time from 50 s to 90 s, there is considerable strain hardening occurred within the target material, as evidenced by the derivation of surface pile-up height. Consequently, the strain hardening decreases the propensity of material ejection in the form of surface pile-up. In the unloading stage, the stress relaxation accompanied with the withdrawal of the indenter leads to a significant recovery of elastic and plastic strains, which accordingly results into a steep rise of pile-up height. However, in the later period of unloading phase, the pile-up deformation behavior keeps stable.

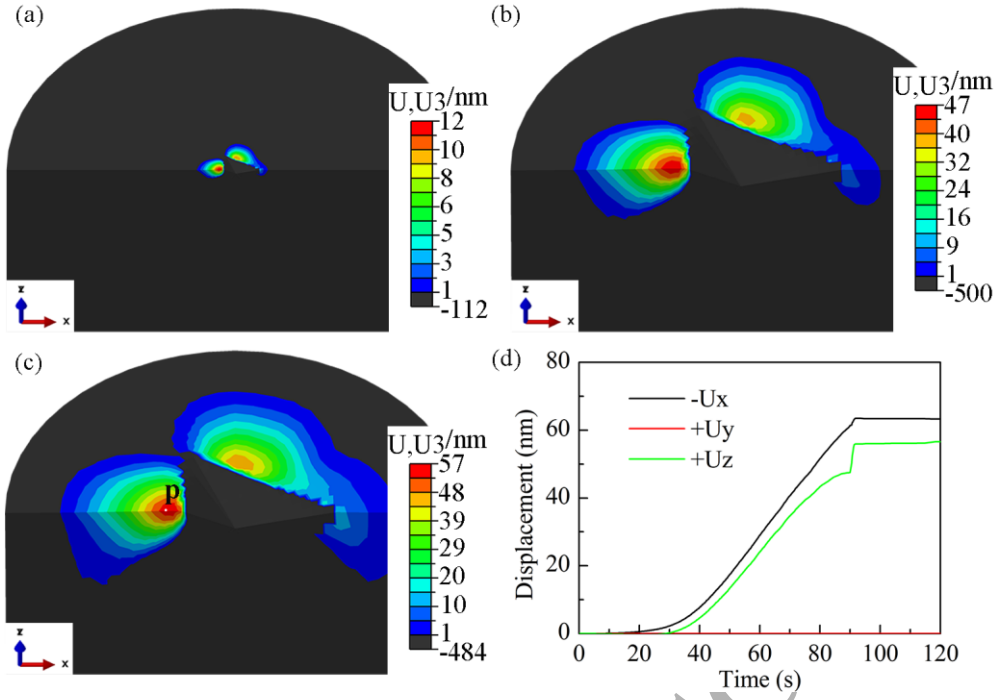

Fig. 6 Surface pile-up evolution of Cu (010) under CPFEM simulation of nanoindentation. Different indentation time: (a) time=20s, (b) time=90s, (c) time=120s. (d) Displacement evolution on the P point.

The symmetry of surface pile-up patterns is heavily dependent on the crystallographic orientation of target material due to activated slip system. Fig. 7(a) illustrates the schematic diagram of 12 slip systems for FCC copper, which are also listed in Table. 4. The slip system is only activated until the applied shear stress on the slip plan reaches the CRSS. For the indentation of Cu(010) surface with a spherical indenter, which is able to avoid symmetries others than those of the crystal structure, the primary slip planes C and B intersect with the indented surface. One each slip plane, there are two slip directions activated under indentation, including c1, -c3, b1 and b3 directions. The dislocation slip along the slip directions on the primary glide planes naturally produces excess material in the intersection areas between slip planes and indented surface, which leads to the formation of four-fold symmetry of surface pile-up. At beginning of Berkovich indentation, the indenter can be regarded as a spherical indenter with a tip radius of 30 nm due to the existence of tip radius. Fig. 7(c) shows the surface pile-up pattern of Cu(010) at an ultra-low displacement of 5nm shows perfect four-fold symmetry, which is widely reported in previous experiments and simulations of nanoindentation tests [18, 19, 47].

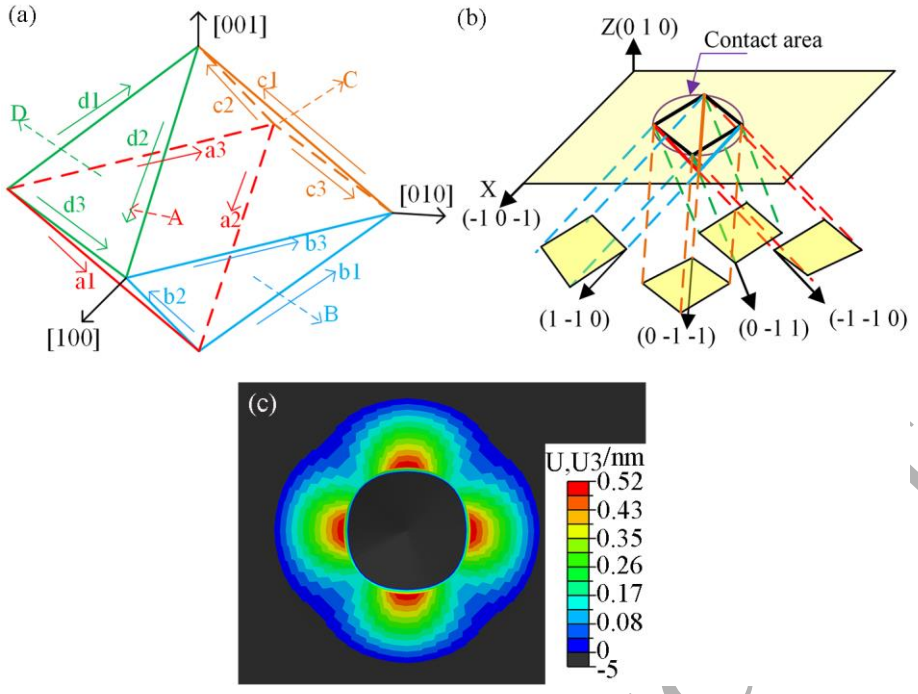

Fig. 7 (a) 12 slip systems in FCC crystal. (b) Slip directions below indented Cu(010) surface. (c) Surface pile-up pattern at a displacement of 5 nm in Berkovich indentation.

Table. 4 12 slip systems composed of four slip planes with three slip directions for FCC crystal

System	a1	a2	a3	b1	b2	b3	c1	c2	c3	d1	d2	d3
Plane	(111)			(11-1)			(-111)			(1-11)		
Direction	[011]	[101]	[110]	[011]	[101]	[110]	[011]	[101]	[110]	[011]	[101]	[110]

However, our CPFEM simulations and experiments of Berkovich nanoindentation jointly show that the surface pile-up deformation behaviour is significantly altered by the indenter geometry. For the Berkovich indenter, the shape of contact area around the indenter is an equilateral triangle that has a specific pattern with a three-fold symmetry. Consequently, the discrete stress distribution pattern results in the deviation of surface pile-up pattern from the activated slip system-dominated four-fold symmetry. In other words, surface pile-up pattern under the Berkovich indentation greatly depends on the relative orientations of crystallographic orientation of indented material and indenter geometry. For instance, both CPFEM simulation data and experimental results demonstrate that the surface pile-up along the TD direction is more pronounced than the other two directions, due to the smaller deviation angle between the vertical line to one of the indenter surfaces and the activated slip direction, as shown in Fig. 4 and Fig. 5.

3.3 Effect of crystallographic orientation

Fig. 8 shows the experimental results and CPFEM simulation data of surface pile-up topographies of Cu(110) and Cu(111) after Berkovich nanoindentation tests. All the parameters used in CPFEM simulations are consistent with those in experiments. Fig. 8 shows that there is an excellent agreement in surface pile-up patterns between experiments and simulations. Firstly, for either Cu(110) or Cu(111), surface pile-up rather than sink-in is formed around the residual impression. Secondly, Cu(110) and Cu(111) has two-fold and three-fold symmetry, respectively. Fig. 9 further plots the surface pile-up height-distance curves along the black lines shown in Fig. 8, which indicates that the surface pile-up distributions by the CPFEM simulations are qualitatively consistent with the experiments.

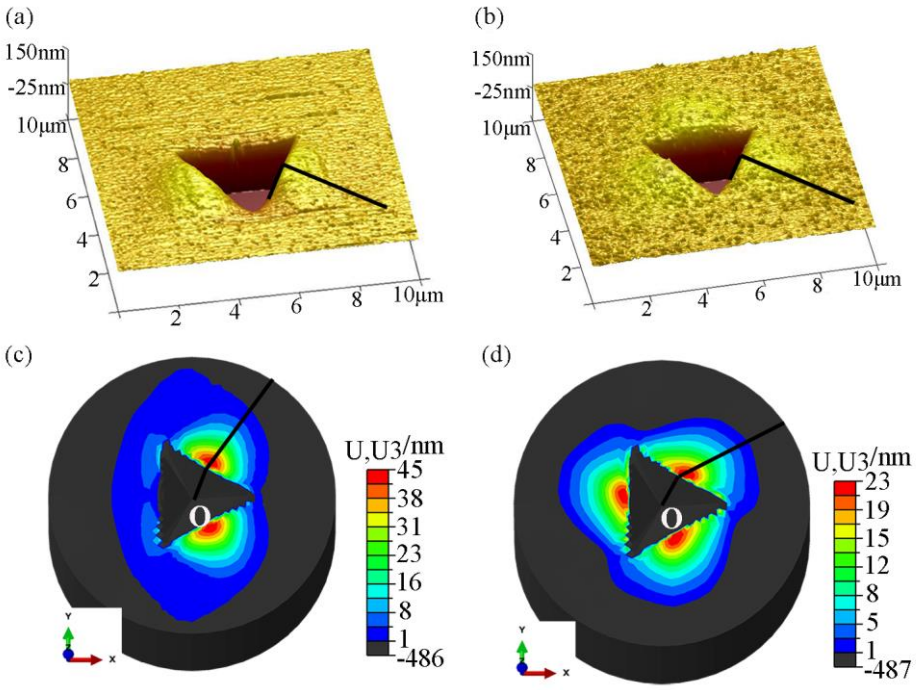

Fig. 8 Surface pile-up topology after Berkovich indentation tests. Experiments: (a) Cu(110) and (b) Cu(111); CPFEM simulations: (c) Cu(110) and (d) Cu(111).

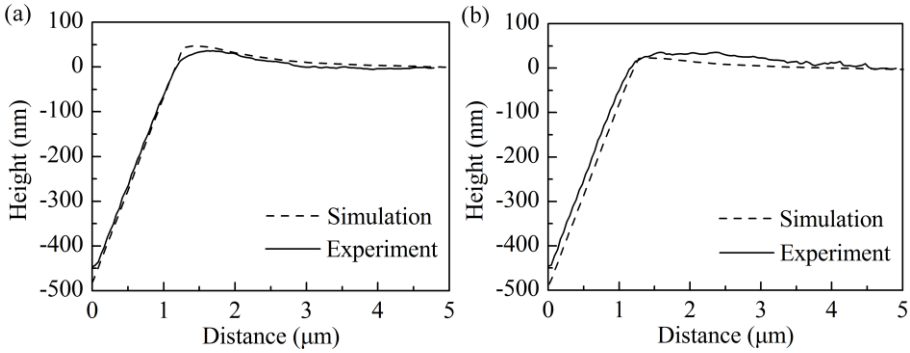

Fig. 9 Experimental and simulated height-distance curves of surface pile-up on (a) Cu(110) and (b) Cu(111).

Fig. 10(a) and (b) shows slip systems below the indented Cu(110) and Cu(111) surface, respectively. For the nanoindentation of Cu(110), there are two primary slip planes B and C intersecting with the indented (110) surface. Accordingly, slip directions contains the b1, b3, c1 and –c3 direction, as shown in Fig. 10(a). However, the angle between the two slip directions b1 and b3, mapping to the intersection face of primary slip plane B with the indented (110) surface, is a small value as 35.26°. Thus, the surface pile-up pattern on Cu(110) reveals a two-fold symmetry. For the nanoindentation of Cu(111), the three-fold symmetry of surface pile-up pattern originates from the intersection of primary slip plane A, B and D along slip direction a2, -b3 and –d1, respectively. Be similar to the analysis of nanoindentation of Cu(010), both experiments and CPFEM simulations of nanoindentation tests of Cu(110) and Cu(111) demonstrate that the surface pile-up evolution has a strong correlation with the relative spatial orientations of indenter geometry and crystallographic orientation of indented material, as indicated in Fig. 8.

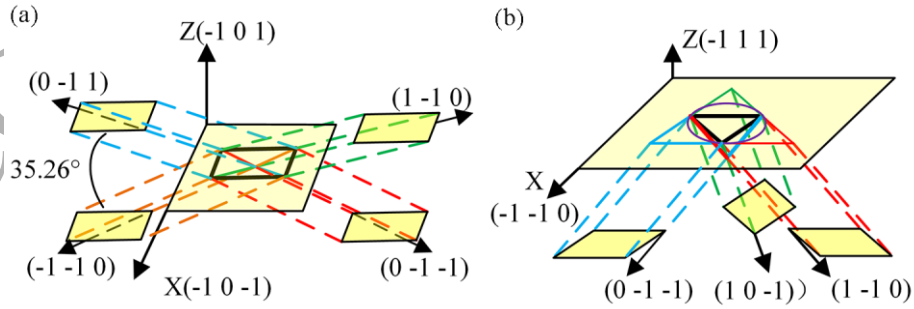

Fig. 10 Slip systems below indented surface during Berkovich nanoindentation of (a) (110) surface and (b) (111) surface.

3.4 Theoretical characterization of surface pile-up

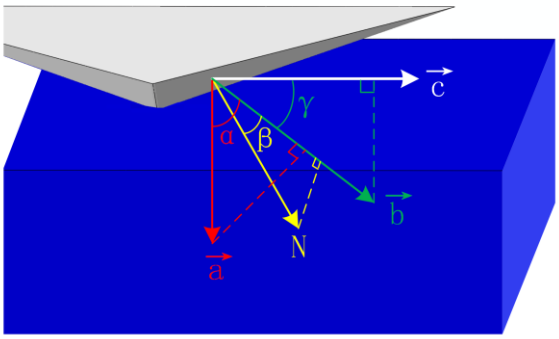

Fig. 11 Schematic model of surface pile-up in Berkovich nanoindentation.

Above CPFEM simulations and experimental investigations jointly demonstrate that the surface pile-up evolution of single crystalline copper in Berkovich nanoindentation tests has a strong correlation with the relative spatial orientation of crystallographic orientation of indented material with respect to indenter geometry. Specifically, different configurations of the relative spatial orientation yield significantly different distribution and numerical value of surface pile-up pattern, which is important for the analysis of anisotropy property of materials. Quantitatively characterization of surface pile-up is of significant importance for facilitating the performance of miro/nano-structures [48].

To rational the theoretical and experimental characterization of surface pile-up deformation behavior, a pile-up density factor, m_p, based on the relative spatial orientation shown in Fig. 11, is proposed in Equ. (4):

$$m_p = \cos(\alpha)\cos(\beta)\cos(\gamma) \tag{4}$$

where α is the angle between the indentation direction $\vec{a}$ and the slip direction of activated slip system $\vec{b}$, β is the angle between the normal direction of indented surface $\vec{N}$ and the slip direction of activated slip system $\vec{b}$, and γ is the angle between the slip direction of activated slip system $\vec{b}$ and the direction of indented surface $\vec{c}$. For a given crystallographic orientation, the slip direction $\vec{b}$ can be also specified according to the stress state [49]. The value of m_p ranges from 0 to 1, and a higher value indicates a higher surface pile-up height. Since the slip direction of activated slip system $\vec{b}$ is intrinsically determined by target material, the proposed pile-up density factor m_p is unique for different crystallographic orientations. And $\vec{c}$ is residing in the indented surface and corresponds to the direction of surface pile up propagation.

According to the Equ. (4), the pile up density factor m_p is closely related to the coupled impacts by both the crystallographic orientation of indented material and the indenter geometry, including indenter contact surface, indented material surface and indentation direction to slip direction, which jointly map to the analysed surface pile-up evolution. The values of m_p of single crystalline Cu with different crystallographic orientations under Berkovich nanoindentation test are calculated and compared with experimentally characterized surface pile-up height. Specifically, Table. 5 lists the values of m_p of Cu(010) along the three lines shown in Fig. 5. For Cu(110) and Cu(111), the values of m_p along the black line shown in Fig. 8 are also presented. According to the height-distance curves for the three lines shown in Fig. 6(b), there is discrepancy in the pile-up height of the three-fold parts along red, green line and blue lines. The red line has the biggest surface pile up of 62.08 nm, which corresponds to the biggest value of the surface pile-up density factor m_p of 0.209. For the other two lines, their values of m_p are the same due to the coupled geometric asymmetry of crystallographic orientation and indenter geometry. Therefore, the proposed pile-up density factor m_p can qualitatively represent the regularity change of surface pile-up in Berkovich nanoindentation tests on the same surface. It should be noted that the proposed pile-up density factor m_p can't distinguish the change of surface pile-up with varying crystallographic orientations, due to the heavily anisotropic characteristics of microscopic plastic deformation behaviour of single crystalline copper.

Table 5 Values of m_p and surface pile-up height along different paths

Grain orientation	PATH	density factor m_p	Pile up height/nm
	Path-red line	0.209	62.08
100	Path-green line	0.194	46.62
	Path-blue line	0.194	46.62
110	Path-black line	0.408	45.04
111	Path-black line	0.431	22.21

.

4 Conclusions

In summary, we perform 3D CPFEM simulations and experiments of Berkovich nanoindentation tests on single crystalline copper with different crystallographic orientations. Specifically, the crystallographic orientation of simulated single crystalline copper is set in the way of Euler angles according to the EBSD characterized values. Mechanical properties of Young's modulus and hardness as well as surface pile-up behavior derived from CPFEM simulations of nanoindentation tests agree well with that from experiments. In particular, both CPFEM simulations and experiments demonstrate that the surface pile-up topography in Berkovich nanoindentation tests is strongly affected by the indenter geometry due to discrete stress distribution pattern, which leads to the modification of the crystallographic orientation-dependent symmetry of surface pile-up. Based on the relative spatial orientation of the crystallographic orientation of indented material with respect to the employed indenter geometry, a pile-up density factor m_p is proposed to qualitatively characterize surface pile-up topography.

Acknowledgements

The authors greatly acknowledge support from the Science Challenge Project (No. TZ2018006), the Fundamental Research Funds for the Central Universities and the National Natural Science Foundation of China (No. 51405106). The authors also acknowledge funding from the German Research Foundation (DFG) (No. 392230176).

Reference

[1] Oliver W C, Pharr G M. Measurement of hardness and elastic modulus by instrumented indentation: Advances in understanding and refinements to methodology[J]. Journal of Materials Research, 2004, 19(1):3-20.

[2] Chrobak D, Kim K H, Kurzydłowski K J, et al. Nanoindentation experiments with different loading rate distinguish the mechanism of incipient plasticity[J]. Applied Physics Letters, 2013, 103(7):32-302.

[3] Suresh S, Giannakopoulos A E. A new method for estimating residual stresses by instrumented sharp indentation[J]. Acta Materialia, 1998, 46(16): 5755-5767.

[4] Wang Y, Raabe D, Klüber C, et al. Orientation dependence of nanoindentation pile-up patterns and of nanoindentation microtextures in copper single crystals[J]. Acta Materialia, 2004, 52(8): 2229-2238.

[5] Tadmor E B, Miller R, Phillips R, et al. Nanoindentation and incipient plasticity[J]. Journal of Materials Research, 1999, 14(6): 2233-2250.

[6] Zhang J, Zhang J, Wang Z, et al. Interaction between phase transformations and dislocations at incipient plasticity of monocrystalline silicon under nanoindentation[J]. Computational Materials Science, 2017, 131: 55-61.

[7] Fischer-Cripps A C. A simple phenomenological approach to nanoindentation creep[J]. Materials Science and Engineering: A, 2004, 385(1-2): 74-82.

[8] Elmustafa A A, Stone D S. Nanoindentation and the indentation size effect: Kinetics of deformation and strain gradient plasticity[J]. Journal of the Mechanics and Physics of Solids, 2003, 51(2): 357-381.

[9] Karthik V, Visweswaran P, Bhushan A, et al. Finite element analysis of spherical indentation to study pile-up/sink-in phenomena in steels and experimental validation[J]. International Journal of Mechanical Sciences, 2012, 54(1): 74-83.

[10] Biener M M, Biener J, Hodge A M, et al. Dislocation nucleation in bcc Ta single crystals studied by nanoindentation[J]. Physical Review B, 2007, 76(16): 165422.

[11] Morris J R, Bei H, Pharr G M, et al. Size effects and stochastic behavior of nanoindentation pop in[J]. Physical review letters, 2011, 106(16): 165502.

[12] Maneiro M A G, Rodríguez J. Pile-up effect on nanoindentation tests with spherical–conical tips[J]. Scripta materialia, 2005, 52(7): 593-598.

[13] Kucharski S, Stupkiewicz S, Petryk H. Surface pile-up patterns in indentation testing of Cu single crystals[J]. Experimental Mechanics, 2014, 54(6): 957-969.

[14] Renner E, Delobelle P, Gaillard Y, et al. Anisotropy and crystal plasticity study of fcc polycrystalline Ni by nanoindentation[C]//21ème Congrès Français de Mécanique (CFM 2013). 2013: 1-6.

[15] Casals O, Forest S. Finite element crystal plasticity analysis of spherical indentation in bulk single crystals and coatings[J]. Computational Materials Science, 2009, 45(3): 774-782.

[16] Casals O, Očenášek J, Alcala J. Crystal plasticity finite element simulations of pyramidal indentation in copper single crystals[J]. Acta materialia, 2007, 55(1): 55-68.

[17] Alcalá Cabrelles J, Casals O, Ocenášek J. Corrigendum to" Micromechanics of pyramidal indentation in fcc metals: Single crystal plasticity finite element analysis"[J]. Journal of the Mechanics and Physics of Solids, 2010, 58(5): 751-751.

[18] Kucharski S, Jarząbek D. Depth dependence of nanoindentation pile-up patterns in copper single crystals[J]. Metallurgical and Materials Transactions A, 2014, 45(11): 4997-5008.

[19] Yao W Z, You J H. Berkovich nanoindentation study of monocrystalline tungsten: a crystal plasticity study of surface pile-up deformation[J]. Philosophical Magazine, 2017, 97(17): 1418-1435.

[20] Renner E, Gaillard Y, Richard F, et al. Sensitivity of the residual topography to single crystal plasticity parameters in Berkovich nanoindentation on FCC nickel[J]. International Journal of Plasticity, 2016, 77: 118-140.

[21] Bolshakov A, Pharr G M. Influences of pileup on the measurement of mechanical properties by load and depth sensing indentation techniques[J]. Journal of materials research, 1998, 13(4): 1049-1058.

[22] Liu M, Lu C, Tieu A K. Crystal plasticity finite element method modelling of indentation size effect[J]. International Journal of Solids and Structures, 2015, 54: 42-49.

[23] Lichinchi M, Lenardi C, Haupt J, et al. Simulation of Berkovich nanoindentation experiments on thin films using finite element method[J]. Thin solid films, 1998, 312(1-2): 240-248.

[24] Brown S B, Kim K H, Anand L. An internal variable constitutive model for hot working of metals[J]. International journal of plasticity, 1989, 5(2): 95-130.

[25] Kalidindi S R, Bronkhorst C A, Anand L. Crystallographic texture evolution in bulk deformation

processing of FCC metals[J]. Journal of the Mechanics and Physics of Solids, 1992, 40(3): 537-569.
[26] Lin G, Havner K S. A comparative study of hardening theories in torsion using the Taylor polycrystal model[J]. International journal of plasticity, 1996, 12(5): 695-718.
[27] Bassani J L, Wu T Y. Latent hardening in single crystals. II. Analytical characterization and predictions[J]. Proc. R. Soc. Lond. A, 1991, 435(1893): 21-41.
[28] Taylor G I. Plastic strain in metals[J]. J. Inst. Metals, 1938, 62: 307-324.
[29] Hill R. A self-consistent mechanics of composite materials[J]. Journal of the Mechanics and Physics of Solids, 1965, 13(4): 213-222.
[30] Meric L, Poubanne P, Cailletaud G. Single crystal modeling for structural calculations: Part 1 - Model Presentation. Journal of Engineering Materials and Technology, 1991, 113: 162–170.
[31] Rice J R. Inelastic constitutive relations for solids: an internal-variable theory and its application to metal plasticity[J]. Journal of the Mechanics and Physics of Solids, 1971, 19(6): 433-455.
[32] Hill R, Rice J R. Constitutive analysis of elastic-plastic crystals at arbitrary strain[J]. Journal of the Mechanics and Physics of Solids, 1972, 20(6): 401-413.
[33] Asaro R J. Crystal plasticity[J]. Journal of applied mechanics, 1983, 50(4b): 921-934.
[34] Asaro R J, Needleman A. Overview no. 42 Texture development and strain hardening in rate dependent polycrystals[J]. Acta metallurgica, 1985, 33(6): 923-953.
[35] Huang Y. A user-material subroutine incroporating single crystal plasticity in the ABAQUS finite element program[M]. Harvard Univ., 1991.
[36] Kysar J. Addendum to "A User-Material Subroutine Incorporating Single Crystal Plasticity in the ABAQUS Finite Element Program" [M]. Harvard Univ., 1997.
[37] Asaro R J, Rice J R. Strain localization in ductile single crystals[J]. Journal of the Mechanics and Physics of Solids, 1977, 25(5): 309-338.
[38] Harvey E, Ladani L, Weaver M. Complete mechanical characterization of nanocrystalline Al–Mg alloy using nanoindentation[J]. Mechanics of Materials, 2012, 52:1-11.
[39] Magee A C, Ladani L. Representation of a microstructure with bimodal grain size distribution through crystal plasticity and cohesive interface modeling[J]. Mechanics of Materials, 2015, 82:1-12.
[40] Choudhury S F, Ladani L. Single Crystal Plasticity Finite Element Analysis of Cu 6 Sn 5, Intermetallic[J]. Metallurgical & Materials Transactions A, 2015, 46(3):1108-1118.
[41] Boeff M. Micromechanical modelling of fatigue crack initiation and growth[J]. 2016.
[42] Pan J, Rice J R. Rate sensitivity of plastic flow and implications for yield-surface vertices[J]. International Journal of Solids and Structures, 1983, 19(11): 973-987.
[43] Hutchinson J W. Bounds and self-consistent estimates for creep of polycrystalline materials[J]. Proc. R. Soc. Lond. A, 1976, 348(1652): 101-127.
[44] Roters F, Eisenlohr P, Hantcherli L, et al. Overview of constitutive laws, kinematics, homogenization and multiscale methods in crystal plasticity finite-element modeling: Theory, experiments, applications[J]. Acta Materialia, 2010, 58(4):1152-1211.
[45] Eidel B. Crystal plasticity finite-element analysis versus experimental results of pyramidal indentation into (0 0 1) fcc single crystal[J]. Acta Materialia, 2011, 59(4): 1761-1771.
[46] Suresh S, Nieh T G, Choi B W. Nano-indentation of copper thin films on silicon substrates[J]. Scripta Materialia, 1999, 41(9):951-957.
[47] Liu M, Lu C, Tieu K A, et al. A combined experimental-numerical approach for determining mechanical properties of aluminum subjects to nanoindentation[J]. Scientific reports, 2015, 5: 15072.

[48] Yan Y, et al. Fabrication of arrayed triangular micro-cavities for SERS substrates using the force modulated indention process [J]. Rsc Advances, 2017, 7(20):11969-11978

[49] Li T L, Gao Y F, Bei H, et al. Indentation Schmid factor and orientation dependence of nanoindentation pop-in behavior of NiAl single crystals[J]. Journal of the Mechanics & Physics of Solids, 2011, 59(6):1147-1162.

CPFEM simulations and experiments of Berkovich nanoindentation tests reveal that the relative spatial orientation between crystallographic orientation of indented material and indenter geometry results into the modification of activated slip system-dominated surface pile-up pattern.

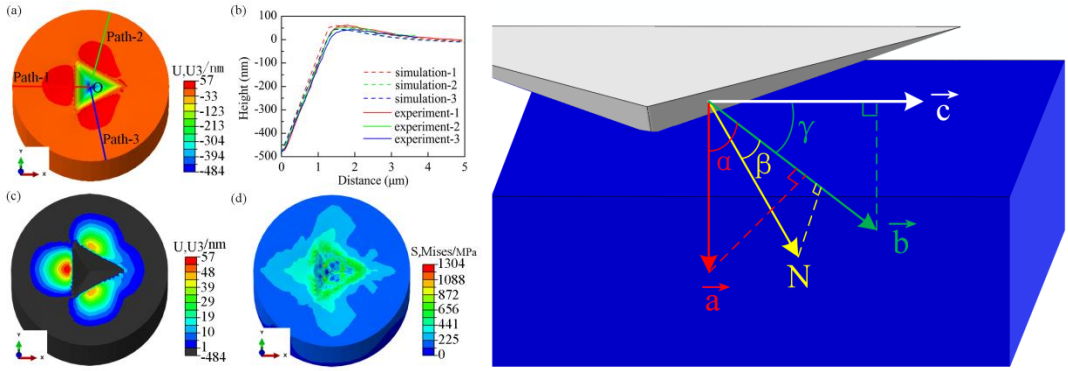

Graphical abstract